Application of the Measurement Integrated Simulation Method to Compressible Fluid Problems

Kentaro Imagawa
Kanako Yasue
Shigeru Kuchi-Ishi

Japan Aerospace Exploration Agency
7-44-1, Jindaiji-Higashi, Chofu, Tokyo 182-8522, JAPAN
Email: imagawa@chofu.jaxa.jp

Abstract

Measurement Integrated Simulation (MIS) is a data assimilation method using the idea of a flow observer. MIS is already used in the analysis of incompressible fluids in biomedical and pipe flows. In this study, a coupled system of a CFD solver and an MIS algorithm was constructed, and an identical twin experiment for the flow field around a 2-dimensional airfoil subject to different boundary conditions was performed. It was found that the MIS reproduced the aerodynamic coefficients of target data even if different boundary conditions are set. The accuracy of MIS was demonstrated, not only for the physical properties used for the assimilation but also for unassimilated properties. In addition, for sample data with random or bias error, the difference between the simulated and sample data achieved by the computation with MIS was much smaller than the difference achieved without MIS.

Key words: Experimental Fluid Dynamics (EFD), Computational Fluid Dynamics (CFD), Data Assimilation, Measurement Integrated Simulation (MIS).

1. Introduction

At the Japan Aerospace Exploration Agency (JAXA), the complementary use of Experimental Fluid Dynamics (EFD) and Computational Fluid Dynamics (CFD) is currently being studied [1]. In flow analysis, EFD and CFD are commonly used. EFD is a direct method to obtain the state of real flow phenomena, and its reliability is ensured by calibration techniques. However, there are differences from real flight condition, such as Reynolds number, the walls and support of the wind tunnel, and model deformation. Moreover, it is impossible to obtain complete information about the flow state both spatially and temporally. On the other hand, CFD provides the full state of

flow phenomena on grid points of the computational domain. However its reliability is always a concern, especially for complicated phenomena such as turbulence, transition, separation, and reacting flow; so validation by experiment is required. These advantages and disadvantages of the two approaches are summarized in Table 1.

A primary aim of EFD/CFD integration is to improve the accuracy and reliability of data by the complementary use of EFD and CFD. Such data assimilation techniques have been employed in many fields. In aerodynamics, 4-dimensional variational assimilation (4D-Var) [2], the extended Kalman filter (EKF) [3], [4], the ensemble Kalman filter (EnKF) [5] and the particle filter (PF) [6] are used. These methods use the error covariance matrices of EFD and CFD to optimize the assimilation parameter. However it is sometimes difficult to estimate precisely the error components in determining the matrix. When 4D-Var or the EKF is used, the reliability of the estimated matrices is a concern. When the EnKF or PF is used, the matrices are estimated by ensemble computation and the computational cost is high.

In maritime engineering, the nudging method is also used to overcome the disadvantages of these methods [7]. The nudging method is a simple method and its computational cost is low because, in contrast to other methods in which the assimilation parameter is optimized from the covariance matrices, this parameter is specified a priori.

Measurement integrated simulation method is a data assimilation method that uses the idea of a flow observer [8]. It is used in the analysis of incompressible fluids in biomedical [9], [10] and pipe [11], [12] flows. The observer algorithm [13] is similar to the Kalman filter [14] in the sense that it is a maximum likelihood estimation method using the error covariance matrices of CFD and EFD. However, it is a method of reproducing EFD data itself and it is also a nudging method since the assimilation parameter is chosen a priori.

In this study, a coupled system of a CFD solver and an MIS algorithm was constructed, and an identical twin experiment, studying the flow field around a 2-dimensional airfoil, was performed to investigate the accuracy and versatility of the method.

Table 1: Advantages and disadvantages of EFD and CFD

	Advantage	Disadvantage
EFD	・A direct way to obtain real flow phenomena ・Reliability is ensured by calibration techniques	・Differences from real flight conditions ・Difficulty in obtaining complete information
CFD	・Provides the full state of flow phenomena	・Reliability is always a concern ・Validation by experiment is required

2. Measurement Integrated Simulation method (MIS)

MIS is a method of integrating measurement and simulation data by applying the idea of a flow observer (Figure 1). This is similar to the EKF, but is a method of reproducing EFD data itself. It is useful for the problem of interpolating missing or immeasurable measurement data. The main feature of MIS, which distinguishes it from other existing observers, is the use of the CFD scheme as a mathematical model of the physical flow.

The governing equations of the CFD model are generally written as

$$\frac{d\mathbf{Q}_N}{dt} = f\left(\mathbf{Q}_N\right) \tag{1}$$

where $\mathbf{Q}_N$ is a 5N-dimensional conservative vector

$$\mathbf{Q}_N = \left(\mathbf{Q}_1^T \quad \mathbf{Q}_2^T \quad \cdots \quad \mathbf{Q}_i^T \quad \cdots \quad \mathbf{Q}_N^T\right)^T \tag{2}$$

$$\mathbf{Q}_i = \left(\rho_i \quad (\rho u)_i \quad (\rho v)_i \quad (\rho w)_i \quad e_i\right)^T \tag{3}$$

and N and $\mathbf{Q}_i$ are the number of grid points and the conservative vector at grid i, respectively. When the vector constructed from measurement data is denoted by $\mathbf{y}$, the basic equation of MIS is

$$\frac{d\mathbf{Q}_N}{dt} = f\left(\mathbf{Q}_N\right) + \mathrm{K}\left(\mathbf{y} - h\left(\mathbf{Q}_N\right)\right) \tag{4}$$

where the second term is the additional term of MIS derived from the difference between EFD and CFD. Function *h* is called the "observation function" and is the relation between the measurement vector **y** of EFD and the conservative vector $\mathbf{Q}_N$ of CFD. K is called the "feedback gain matrix". This matrix is constructed from the assimilation parameter. In MIS, the assimilation parameter is not optimized from the error covariance matrices, as it is in the EKF or EnKF. In previous studies of MIS, the matrix was designed by trial and error based on physical considerations, because the theory of the observer cannot be directly applied [15], [16].

In this study, the feedback matrix is designed using the Jacobi matrix H of the nonlinear observation function *h*. The details are given in Section 3.3.

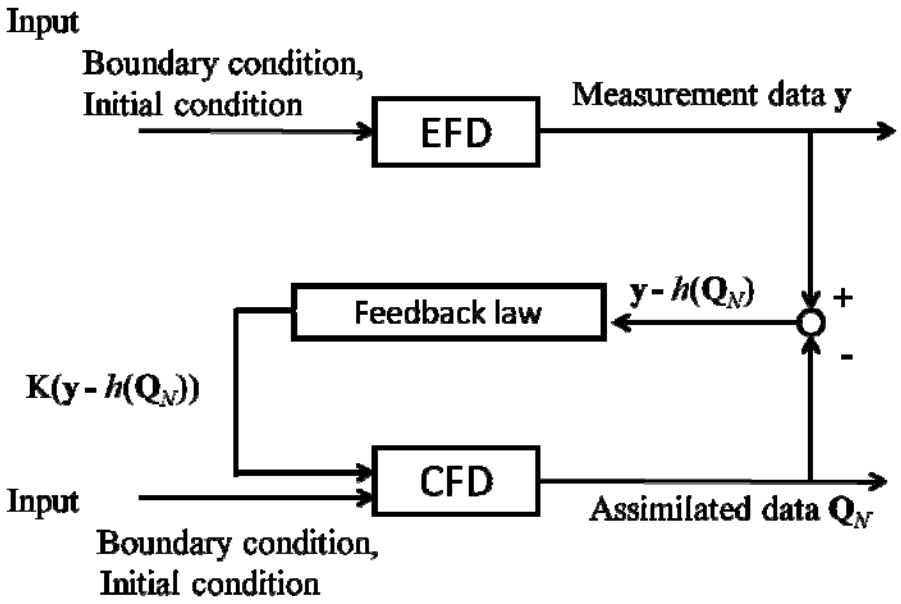

Figure 1: Block diagram of MIS

3. Numerical Experiment

In this section, a coupled system of a high-speed CFD solver (FaSTAR)[17], and MIS is described, and an identical twin experiment investigated flow field around a 2-dimensional airfoil with different boundary conditions is discussed. First, the twin experiment used in this study is explained briefly. Then, the computational conditions are given and the corresponding feedback matrix is derived.

3.1. Twin experiment

Twin experiments are a method of numerical experiment commonly used for benchmark tests of data assimilation techniques. This method uses pseudo-measurement data derived from simulation instead of measurements.

Figure 2 shows a schematic diagram of the twin experiment. The target data is original CFD data, and the sample data is created by adding an error component to the target data. Generally, the benchmark test of the integrated

analysis system is comparing comparison with the target data. The benchmark in this study is, however, a comparison with the sample data since MIS is a method of reproducing sample data.

The procedure of the twin experiment is as follows.

(1) Produce target data according to specified boundary conditions.
(2) Produce sample data by adding artificial error components to the target data.
(3) Perform integrated analysis with varying boundary conditions by regarding the sample data as measurement data.
(4) Compare the integrated analysis data with the sample data.

3.2. Numerical conditions

The twin experiment deals with flow field around a 2-dimensional airfoil as shown in Fig. (3). The Mach number of the uniform flow is 0.8. The flow field in this study is assumed to be steady, hence the integrated data are obtained as an asymptotic solution of Eq. (4). The flow chart of the algorithm is shown in Fig. (4).

In the twin experiment, the angle of attack in the target data is 3 degrees, and integrated computation is made using intentionally different angles of attack. The sample cases in the present experiment are shown in Table 2. The sample data is the velocity field over the whole computational domain. In this study, three types of sample data are employed: (1) data without measurement error (exactly same as the target data); (2) data with random errors of 1%, 2%, 5%, or 10%; and (3) data with bias error of 1%, 2%, 5%, or 10%. All computations were done using the JAXA Super computer System (JSS).

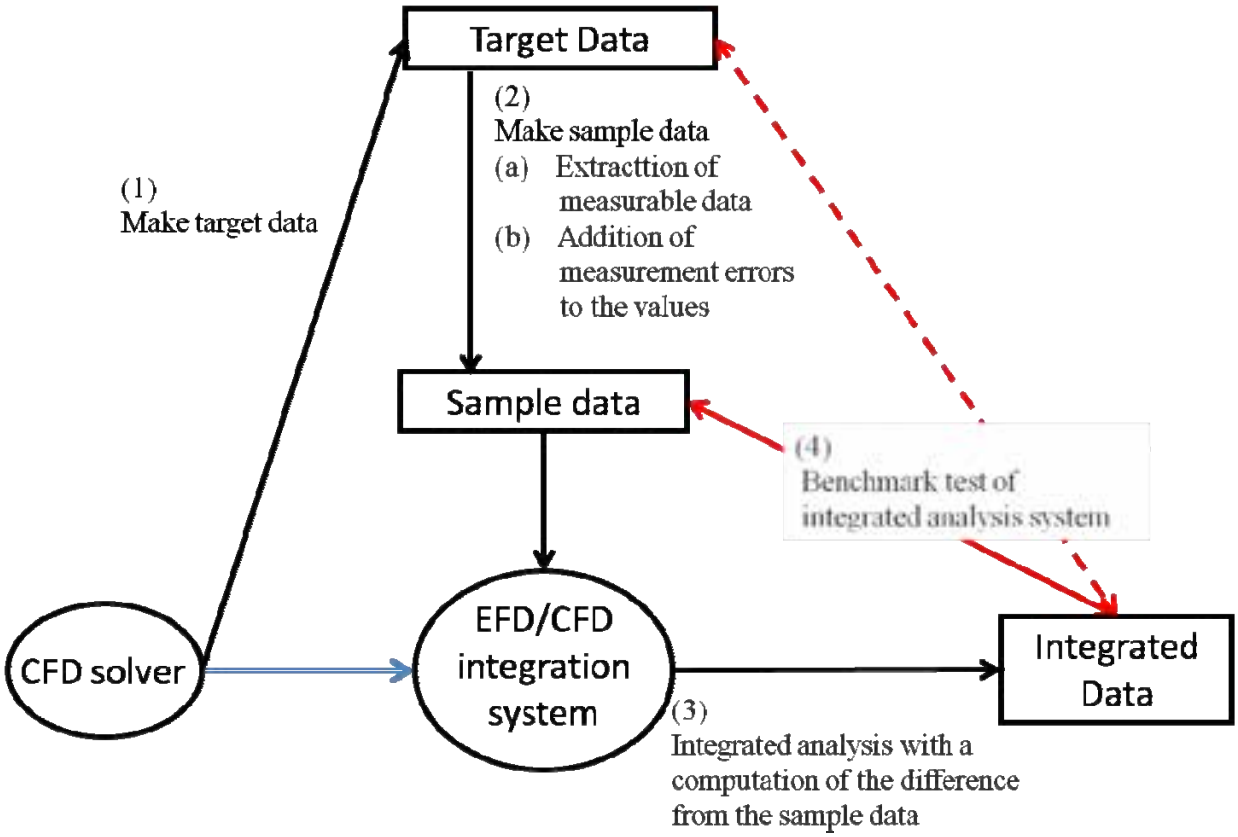

Figure 2: Schematic diagram of twin experiment

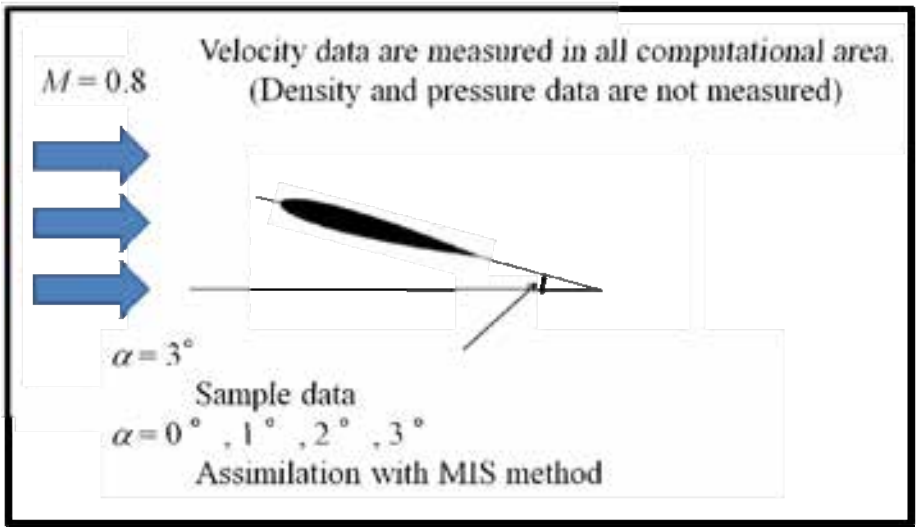

Figure 3: Setup of this twin experiment

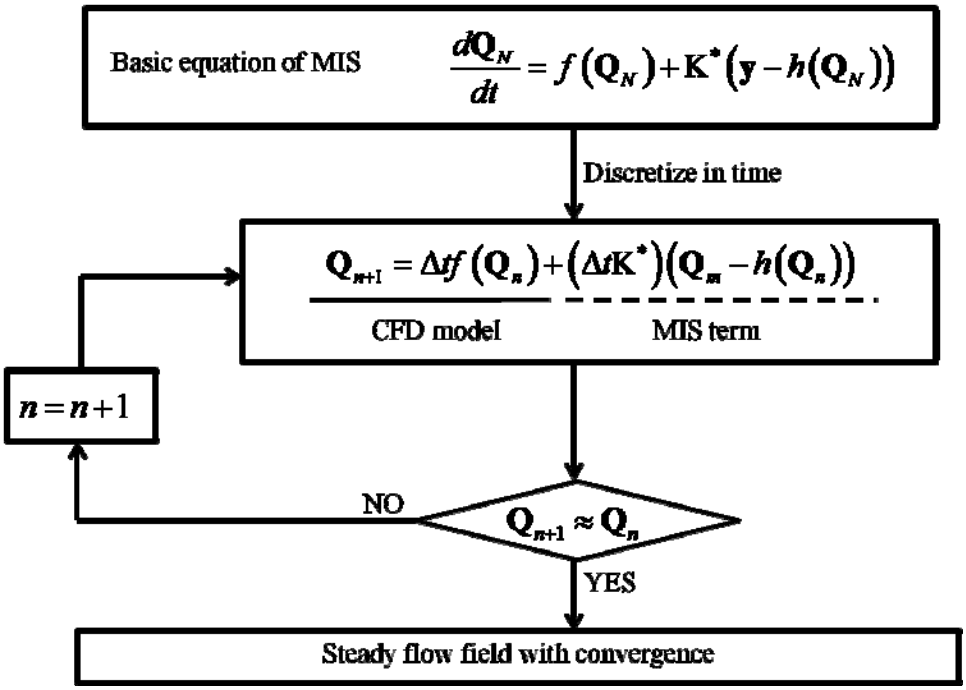

Figure 4: Flow chart of EFD/CFD integrated computation of MIS

Table 2: Sample cases of twin experiment

	Angle of attack (AoA)
Case (1)	0°
Case (2)	1°
Case (3)	2°
Case (4)	3° (Same AoA as the target data)

3.3. Feedback gain matrix design

In this study, the feedback gain matrix K in Eq. (4) is derived as a pseudo-inverse matrix of the Jacobi matrix of the observation function.

If the velocity components are employed as measurement data, **y** in Eq. (4) is

$$\mathbf{y} = \begin{pmatrix} \mathbf{y}_1^T & \mathbf{y}_1^T & \cdots & \mathbf{y}_i^T & \cdots & \mathbf{y}_N^T \end{pmatrix}^T, \tag{5}$$

$$\mathbf{y}_i = \begin{pmatrix} u_i & v_i \end{pmatrix}^T, \tag{6}$$

and the Jacobi matrix H of the observation function h is

$$\mathrm{H} = \frac{\partial \mathbf{y}}{\partial \mathbf{Q}_N} = diag\begin{pmatrix} \mathrm{H}_1 & \mathrm{H}_2 & \cdots & \mathrm{H}_i & \cdots & \mathrm{H}_N \end{pmatrix} \tag{7}$$

$$\begin{aligned} \mathrm{H}_i = \frac{\partial \mathbf{y}_i}{\partial \mathbf{Q}_i} &= \frac{\partial \begin{pmatrix} u_i & v_i \end{pmatrix}^T}{\partial \begin{pmatrix} \rho_i & (\rho u)_i & (\rho v)_i & (\rho w)_i & e_i \end{pmatrix}^T} \\ &= \frac{\partial \begin{pmatrix} u_i & v_i \end{pmatrix}^T}{\partial \begin{pmatrix} \rho_i & u_i & v_i & w_i & p_i \end{pmatrix}^T} \frac{\partial \begin{pmatrix} \rho_i & u_i & v_i & w_i & p_i \end{pmatrix}^T}{\partial \begin{pmatrix} \rho_i & (\rho u)_i & (\rho v)_i & (\rho w)_i & e_i \end{pmatrix}^T} = \mathrm{M}_i \mathrm{L}_i \end{aligned} \tag{8}$$

where

$$\begin{aligned} \mathrm{L}_i &= \frac{\partial \begin{pmatrix} \rho_i & u_i & v_i & w_i & p_i \end{pmatrix}^T}{\partial \begin{pmatrix} \rho_i & (\rho u)_i & (\rho v)_i & (\rho w)_i & e_i \end{pmatrix}^T} \\ &= \begin{pmatrix} 1 & 0 & 0 & 0 & 0 \\ -\frac{u_i}{\rho_i} & \frac{1}{\rho_i} & 0 & 0 & 0 \\ -\frac{v_i}{\rho_i} & 0 & \frac{1}{\rho_i} & 0 & 0 \\ -\frac{w_i}{\rho_i} & 0 & 0 & \frac{1}{\rho_i} & 0 \\ \frac{1}{2}(\gamma-1)\left(u_i^2+v_i^2+w_i^2\right) & -(\gamma-1)u_i & -(\gamma-1)v_i & -(\gamma-1)w_i & \gamma-1 \end{pmatrix}. \end{aligned} \tag{9}$$

and

$$\mathrm{M}_i = \frac{\partial \begin{pmatrix} u_i & v_i \end{pmatrix}^T}{\partial \begin{pmatrix} \rho_i & u_i & v_i & w_i & p_i \end{pmatrix}^T} = \begin{pmatrix} 0 & 1 & 0 & 0 & 0 \\ 0 & 0 & 1 & 0 & 0 \end{pmatrix}. \tag{10}$$

Further, L_i is the transformation matrix from conservative vector to primitive vector. L_i^{-1}, the inverse matrix of L_i, is the transformation matrix from primitive vector to conservative state vector which is given by

$$\mathrm{L}_i^{-1} = \frac{\partial\left(\rho_i \quad (\rho u)_i \quad (\rho v)_i \quad (\rho w)_i \quad e_i\right)^T}{\partial\left(\rho_i \quad u_i \quad v_i \quad w_i \quad p_i\right)^T} = \begin{pmatrix} 1 & 0 & 0 & 0 & 0 \\ u_i & \rho_i & 0 & 0 & 0 \\ v_i & 0 & \rho_i & 0 & 0 \\ w_i & 0 & 0 & \rho_i & 0 \\ \frac{1}{2}\left(u_i^2+v_i^2+w_i^2\right) & \rho_i u_i & \rho_i v_i & \rho_i w_i & \frac{1}{\gamma-1} \end{pmatrix}, \tag{11}$$

and M_i^{-1}, the pseudo-inverse matrix of M_i, is

$$\mathrm{M}_i^{-1} = \begin{pmatrix} 0 & 1 & 0 & 0 & 0 \\ 0 & 0 & 1 & 0 & 0 \end{pmatrix}^T \tag{12}$$

Then, H^*, the pseudo-inverse matrix of H, is

$$\mathrm{H}^* = diag\left(\mathrm{H}_1^* \quad \mathrm{H}_2^* \quad \cdots \quad \mathrm{H}_i^* \quad \cdots \quad \mathrm{H}_N^*\right) \tag{13}$$

$$\mathrm{H}_i^* = \mathrm{L}_i^{-1}\mathrm{M}_i^* = \begin{pmatrix} 0 & \rho_i & 0 & 0 & \rho_i u_i \\ 0 & 0 & \rho_i & 0 & \rho_i v_i \end{pmatrix}^T \tag{14}$$

In this experiment, the feedback gain matrix K^* is designed using H^* and is given by

$$\mathrm{K}^* = k\mathrm{H}^* \tag{15}$$

where k is a stability parameter. In previous studies, this parameter was determined by trial and error. These studies indicated that this parameter depends on the time increment Δt of the time-marching scheme from the viewpoint of scaling. When the first order implicit scheme is used as the time-marching algorithm, the stabilization condition becomes[18]

$$k \le \frac{1}{\Delta t} \tag{16}$$

Hence, in the present study, the parameter k is set to

$$k = \frac{1}{\Delta t} \tag{17}$$

Finally we obtain the feedback gain matrix K^* as

$$\mathrm{K}^* = diag\left(\mathrm{K}_1^* \quad \mathrm{K}_2^* \quad \cdots \quad \mathrm{K}_i^* \quad \cdots \quad \mathrm{K}_N^*\right) \tag{18}$$

$$\mathrm{K}_i^* = \frac{1}{\Delta t}\mathrm{H}_i^* = \frac{1}{\Delta t}\begin{pmatrix} 0 & \rho_i & 0 & 0 & \rho_i u_i \\ 0 & 0 & \rho_i & 0 & \rho_i v_i \end{pmatrix}^T \tag{19}$$

4. Results and Discussion

First, we discuss the results for the case using the sample data without error. The comparisons of the drag coefficients C_D and lift coefficients C_L with and without MIS are shown in Table 3. The computation without MIS is equivalent to a simple CFD computation, and its difference from the target data becomes large as the angle of attack recedes from the target value. On the other hand, the computations with MIS successfully reproduce the sample data.

The accuracy of the MIS method can be evaluated by using the norms of the difference between two sets of data

$$I_\rho^{S-M} = \sqrt{\frac{1}{N}\sum_{i=1}^{N}\left(\rho_i^{sample} - \rho_i^{MIS}\right)^2} \tag{20}$$

$$I_u^{S-M} = \sqrt{\frac{1}{2N}\sum_{i=1}^{N}\left\{\left(u_i^{sample} - u_i^{MIS}\right)^2 + \left(v_i^{sample} - v_i^{MIS}\right)^2\right\}} \tag{21}$$

$$I_p^{S-M} = \sqrt{\frac{1}{N}\sum_{i=1}^{N}\left(p_i^{sample} - p_i^{MIS}\right)^2} \tag{22}$$

$$I_\rho^{S-C} = \sqrt{\frac{1}{N}\sum_{i=1}^{N}\left(\rho_i^{sample} - \rho_i^{CFD}\right)^2} \tag{23}$$

$$I_u^{S-C} = \sqrt{\frac{1}{2N}\sum_{i=1}^{N}\left\{\left(u_i^{sample} - u_i^{CFD}\right)^2 + \left(v_i^{sample} - v_i^{CFD}\right)^2\right\}} \tag{24}$$

$$I_p^{S-C} = \sqrt{\frac{1}{N}\sum_{i=1}^{N}\left(p_i^{sample} - p_i^{CFD}\right)^2} \tag{25}$$

where the upper subscript *sample* denotes the sample data, *CFD* the result without MIS, and *MIS* the computation with MIS. The subscript *i* is the grid index and *N* is the number of grid points.

Table 4 shows a comparison of the norms derived from Eqs. (20)-(25). Since the velocity data are employed as the target data, in all cases, the value of velocity norm obtained with MIS is much smaller than that obtained without MIS. On the other hand, for the norms for density and pressure obtained with MIS are also much smaller than those obtained without MIS. This means that the present method can even reproduce physical properties that are not assimilated directly. Figure 5 shows pressure contours in Case (1). Figure 5 (b) shows the computation without MIS and of course the distribution is different from that of the target data. On the contrary, as can be seen in Fig. 5 (c), an almost identical result is obtained from the computation with MIS.

Next we consider the results obtained when random and bias errors are introduced. This is to confirm the validity of the MIS method even if the sample data includes a typical amount of uncertainty. The sample data including random or bias errors are derived from the target data as

Table 3: Comparison of aerodynamic coefficients with and without MIS

	C_D		C_L	
	Without MIS	With MIS	Without MIS	With MIS
Case (1)	0.022518	0.030731	-0.000230	0.260082
Case (2)	0.023963	0.030776	0.142230	0.260634
Case (3)	0.027097	0.030815	0.221770	0.261135
Target data	0.030849		0.261591	

Table 4: Differences between the results of calculations with and without MIS for the sample data without errors

	Without MIS			With MIS		
	I_ρ^{S-C}	I_u^{S-C}	I_p^{S-C}	I_ρ^{S-M}	I_u^{S-M}	I_p^{S-M}
Case (1)	0.05255	0.1492	0.04382	0.006436	0.003614	0.004457
Case (2)	0.03925	0.1132	0.03355	0.004305	0.002409	0.002969
Case (3)	0.02305	0.06211	0.01903	0.002181	0.001204	0.001485

$$\mathbf{y}_i^{random} = \left(1 + r_i\right)\mathbf{y}_i^{target} \tag{26}$$

$$\mathbf{y}_i^{bias} = (1 + b)\mathbf{y}_i^{target} \tag{27}$$

where r_i is a random number chosen so that the level of uncertainty attains a specified value. Similarly, b is a constant which represents the bias error component. A total of 4 cases, with levels of uncertainty of 1%, 2%, 5%, and 10%, are considered both for random error and bias error. The results of including random or bias error are shown in Tables 5 and 6, respectively. In both cases, the difference norms for the computation with MIS are much smaller than those obtained without MIS.

By solving Eq. (4), MIS reproduces the flow field so that it minimizes the difference from the sample data. Hence, when the sample data exactly satisfies the flow equations, the sample data itself is reproduced. However, if the sample data does not satisfy the flow equations due to the presence of random or bias error, the difference between the sample data and the MIS computation remains. The degree of difference between the MIS and sample data is comparable to that between the target and sample data. The difference becomes large as the error included in the sample data becomes large, as shown in Tables 5 and 6.

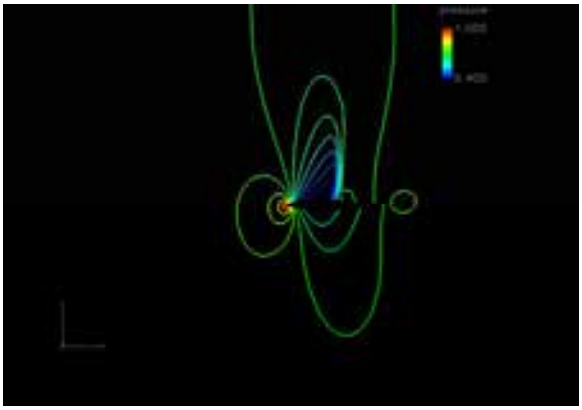

(a) Target data

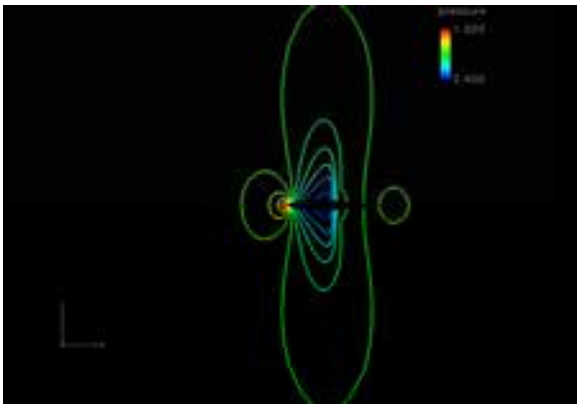

(b) Without MIS

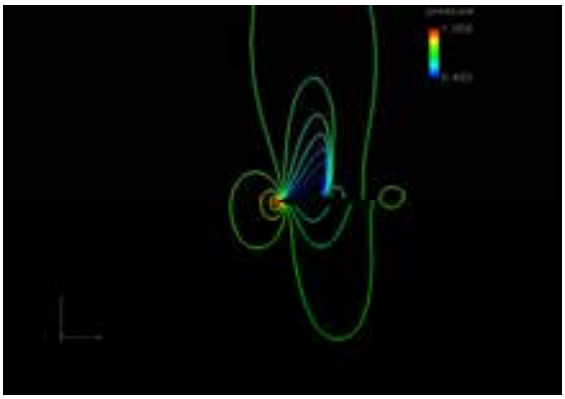

(c) With MIS

Figure 5: Comparison of pressure contours

Finally, we consider the effects of random or bias error on the MIS results for Case (4) in which results that are identical to those of the sample data are expected to be obtained if there is no error in the sample data. Table 7 shows the comparison of the difference norms obtained with random or bias error

$$l_u^{S-T} = \sqrt{\frac{1}{2N}\sum_{i=1}^{N}\left\{\left(u_i^{sample} - u_i^{target}\right)^2 + \left(v_i^{sample} - v_i^{target}\right)^2\right\}} \tag{28}$$

and those obtained by the MIS computation. In both cases, the norm from the MIS computation is comparable to that from the computation with random or bias error. This means that, even if the assimilated data has a series of uncertainties, MIS does not amplify the uncertainty level, and hence, we can say that MIS is a numerically stable approach.

Table 5: Differences between the results of calculations with and without MIS for the sample data including random errors

(a) 1%

	Without MIS	With MIS
	l_u^{S-C}	l_u^{S-M}
Case (1)	0.1497	0.0055
Case (2)	0.1136	0.0040
Case (3)	0.0625	0.0027
Case (4)	0.0041	0.0022

(b) 10%

	Without MIS	With MIS
	l_u^{S-C}	l_u^{S-M}
Case (1)	0.1587	0.0212
Case (2)	0.1236	0.0208
Case (3)	0.0765	0.0206
Case (4)	0.0413	0.0206

Table 6: Differences between the results of calculations with and without MIS for the sample data including bias errors

(a) 1%

	Without MIS	With MIS
	l_u^{S-C}	l_u^{S-M}
Case (1)	0.1502	0.0058
Case (2)	0.1141	0.0041
Case (3)	0.0630	0.0028
Case (4)	0.0072	0.0023

(b) 10%

	Without MIS	With MIS
	l_u^{S-C}	l_u^{S-M}
Case (1)	0.1730	0.0176
Case (2)	0.1396	0.0172
Case (3)	0.0980	0.0169
Case (4)	0.0718	0.0168

Table 7: Effect of size of random or bias error in calculations with and without MIS

(a) Random error

Level of uncertainty	Without MIS	With MIS
	l_u^{S-T}	l_u^{S-M}
1%	0.0030	0.0022
2%	0.0059	0.0042
5%	0.0147	0.0104
10%	0.0295	0.0206

(b) Bias error

Level of uncertainty	Without MIS	With MIS
	l_u^{S-T}	l_u^{S-M}
1%	0.0051	0.0023
2%	0.0102	0.0042
5%	0.0256	0.0100
10%	0.0512	0.0168

5. Conclusions

Measurement Integrated Simulation (MIS) is a data assimilation method that uses the idea of a flow observer and has already been applied to the analysis of incompressible fluids in biomedical and pipe flows. In this study, a coupled system of a CFD solver and MIS was constructed, and an identical twin experiment studying the flow field around a 2-dimensional airfoil with different boundary conditions was performed. The velocity data for all parts of the computational domain were used as the target data. The target data were used as "sample data without error" and further sample data was created by adding random and bias error components. In cases using the sample data without error, it was found that the MIS reproduced the aerodynamic coefficients of target data even if we set different boundary conditions. Based on the evaluation of the L2 norms for the differences between the target data and the simulated data, the accuracy of the MIS method was demonstrated, not only for the physical properties used for the assimilation but also for unassimilated properties. Also, for the cases involving sample data with random or bias error, the difference between the simulated and target data achieved by the computation with MIS was much smaller than the difference achieved without MIS.

MIS is a nudging method and has a computational cost comparable with single CFD. Therefore, in future research, we will apply this method to 3-dimensional problems using actual measurement data, for example, collected by particle image velocimetry.

Acknowledgments

The authors thank Dr. Atsushi Hashimoto who provided the CFD solver FaSTAR. We also thank Dr. Kazuyuki Nakakita, Dr Hiroyuki Kato, and Mr. Makoto Ueno for their helpful comments and suggestions.

References

[1] Watanabe S., Kuchi-Ishi S., Aoyama T.; A Prototype System towards EFD/CFD Integration: Digital/Analog Hybrid Wind Tunnel, *27th Congress of International Council of the Aeronautical Science*, 2010, http://www.icas.org/ICAS_ARCHIVE_CD1998-2010/ICAS2010/ABSTRACTS/244.HTM

[2] Misaka T., Ogasawara T., Obayashi S., Yamada I., Okuno Y.; Assimilation Experiment of Lidar Measurements for Wake Turbulence, *Journal of Fluid Science and Technology*, 3(4), pp.512-518, 2008.

[3] Chowdhary G., Jategaonkar R.; Aerodynamic Parameter Estimation from Flight Data Applying Extended and Unscented Kalman filter, *Aerospace Science and Technology*, 14 (2), pp.106-117, 2010.

[4] Suzuki T., Ji H., Yamamoto F.; Reduced-order Kalman-Filtered Hybrid Simulation Combining PTV and DNS,*9th International Symposium on Particle Image Velocimetry*, p. 118, 2011.

[5] Kato H., Obayashi S., Integration of CFD and Wind Tunnel by Data Assimilation, *Journal of Fluid Science and Technology*, 6 (5), pp.717-728,2011.

[6] Imagawa K., Yasue K., Kuchi-Ishi S.; Identification of flow condition around a 2-dimensional airfoil using data assimilation, *43th Fluid Dynamics Conference/ Aerospace Numerical Simulation Symposium 2011*, 2A12 (in Japanese).

[7] Hoke, J., Anthes, R. A.; The initialization of numerical models by a dynamic initialization technique, *Monthly Weather Review*, 104, 1551- 1556, 1976.

[8] Hirose N., Kawamura H., Lee H. J., Yoon J. H., Sequential Forecasting of the Surface and Subsurface Conditions in the Japan Sea, *Journal of Oceanography*, Vol. 63, pp. 467 to 481, 2007

[9] Hayase T, Hayashi S.; State estimator of flow as an integrated computational method with the feedback of online experimental measurement. *Trans. ASME J. Fluids Eng*. 119(4), pp.814–22, 1997.

[10] Funamoto K, Hayase T, Saijo Y, Yambe T.; Numerical study on variation of feedback methods in ultrasonic-measurement- integrated simulation of blood flow in the aneurysmal aorta, *JSME Int. J. Ser C*, 49(1), pp.144–55, 2006.

[11] Funamoto K, Hayase T, Saijo Y, Yambe T.; Numerical Analysis of Effects of Measurement Errors on Ultrasonic-Measurement-Integrated Simulation, *IEEE Trans. Biomedical Engineering*, 58(3), pp.653-663, 2011.

[12] Imagawa K., Hayase T.; Numerical experiment of measurement- integrated simulation to reproduce turbulent flows with feedback loop to dynamically compensate the solution using real flow information, *Computers and Fluids*, 39 (11), pp.1439-1450, 2010.

[13] Nakao M., Kawashima K., Kagawa T.: Application of MI Simulation Using a Turbulent Model for Unsteady Orifice Flow, Journal of Fluids Engineering, 131(11), pp.111401-111409, 2009.

[14] Luenberger D. G.: Observing the State of a Linear System, *IEEE Trans. Military Electronics*, 8(2), pp.74-80, 1964.

[15] Kalman R. E.: A New Approach to Linear Filtering and Prediction Problems, *Trans. ASME*, 82(D), pp.35-45, 1960.

[16] Imagawa K., Hayase T.: Eigenvalue analysis of linearized error dynamics of measurement integrated flow simulation, *Computers and Fluids*, 39(10), pp.1796-1803, 2010.

[17] Hashimoto A., Murakami K., and Aoyama, T, JAXA Digital/Analog Hybrid Wind Tunnel: Development of Digital Wind Tunnel, *JAXA-SP-09-003*, 2010.

[18] Hayase T., Imagawa K., Funamoto K., Shirai A.: Stabilization of Measurement- Integrated Simulation by Elucidation of Destabilizing Mechanism, *Journal of Fluid Science and Technology*, 5(3), pp.632-647, 2010.